The response of the ionospheric peak electron density (NmF2) to solar activity)

Vaishnav, R.[1,✉], Jacobi, Ch.[1], Schmölter, E.[2], Berdermann, J.[2]
Codrescu, M.[3], Dühnen, H.[2]

[1] *Institute for Meteorology, Leipzig University, Stephanstr. 3, 04103 Leipzig, Germany*
[2] *German Aerospace Center, Kalkhorstweg 53, 17235 Neustrelitz, Germany*
[3] *Space Weather Prediction Centre, National Oceanic and Atmospheric Administration, Boulder, Colorado, USA*
✉*e-mail: rajesh_ishwardas.vaishnav@uni-leipzig.de*

Summary: The ionospheric peak electron density NmF2, simulated with the Coupled Thermosphere Ionosphere Plasmasphere electrodynamics (CTIPe) model was used to study the ionospheric response to solar flux in years of low (2008) and high (2013) solar activity. The CTIPe NmF2 was compared to the Whole Atmosphere Community Climate Model with Thermosphere and Ionosphere Extension (WACCM-X) and the Constellation Observing System for Meteorology, Ionosphere, and Climate (COSMIC) NmF2 in March and July of 2008 and 2013. The comparison shows that the CTIPe NmF2 is lower than the COSMIC and WACCM-X NmF2. Both models successfully reproduce the semi-annual variations seen in the COSMIC observations. Analysis of the 27-day variations of the CTIPe NmF2 shows that the midnight NmF2 deviations are stronger than the midday deviations. In addition, at low solar activity, the 27-day variations of NmF2 are larger in the Southern Hemisphere, while at high solar activity, the 27-day variations of NmF2 are larger at the equator and in the Northern Hemisphere.

An ionospheric delay was estimated with CTIPe simulated NmF2 at the 27-day solar rotation period during low and high solar activity. During low (high) solar activity, an ionospheric delay of about 12 (34) hours is predicted indicating an increasing ionospheric delay with solar activity.

Zusammenfassung: Die maximale ionosphärische Elektronendichte NmF2, die mit dem Coupled Thermosphere Ionosphere Plasmasphere electrodynamics (CTIPe) Modell simuliert wurde, wurde zur Untersuchung der ionosphärischen Reaktion in Jahren mit geringer (2008) und hoher (2013) Sonnenaktivität verwendet. CTIPe vorhergesagte NmF2 wurde mit derjenigen des Whole Atmosphere Community Climate Model with Thermosphere and Ionosphere Extension (WACCM-X) und Messwerten des Constellation Observing System for Meteorology, Ionosphere, and Climate (COSMIC) im März und Juli der Jahre 2008 und 2013 verglichen. Der Vergleich zeigt, dass NmF2 aus CTIPe geringer ist als das COSMIC gemessene und von WACCM-X simulierte. Beide Modelle reproduzieren erfolgreich die von COSMIC beobachteten halbjährlichen Schwankungen. Die Analyse der 27-tägigen Schwankungen des CTIPe NmF2 zeigt, dass die mitternächtlichen NMF2-Abweichungen stärker sind als diejenigen am Mittag. Außerdem sind bei geringer Sonnenaktivität die 27-Tage-Abweichungen von NmF2 in der

Südhemisphäre größer, während bei hoher Sonnenaktivität die 27-Tage-Abweichungen von NmF2 am Äquator und in der Nordhemisphäre größer sind.

Die ionosphärische Verzögerung während geringer und hoher Sonnenaktivität wurde für die 27-tägige Sonnenrotation mit CTIPe simuliert. Bei geringer (hoher) Sonnenaktivität wird eine ionosphärische Verzögerung von etwa 12 (34) Stunden beobachtet, was auf eine zunehmende ionosphärische Verzögerung mit zunehmender Sonnenaktivität hinweist.

1 Introduction

The thermospheric and ionospheric parameters, in particular the total electron content (TEC) and the peak electron density of the F2 region (NmF2), are mainly controlled by transport processes, photoionization and photodissociation of the main species O, O_2 and N_2 and depend on the intensity of incident extreme ultraviolet (EUV) and UV radiation from the Sun on various time scales, including the well-understood period of quasi-solar rotation (SR) and the 11-year solar cycle (SC) or longer (e.g. Jakowski et al., 1991; Afraimovich et al., 2008; Liu and Chen, 2009; Chen et al., 2015). Variations in solar irradiance are observed by satellites, and they have significant implications for the peformance of global navigation satellite systems (GNSS) and satellite communications. Therefore, it is important to characterise the influence of solar radiation on the thermosphere-ionosphere region. EUV can vary by more than a factor of 2 between solar minimum and maximum.

Since continuous observations of the whole EUV spectrum were not available prior to the TIMED/SEE mission starting in 2002 (Woods et al., 2000), solar EUV proxies, e.g., the F10.7 solar radio flux at 10.7 cm (Tapping, 2013) and Mg-II index, are used to represent solar activity.

The 27-day variations in solar flux are significantly modulated and amplified at higher solar activity compared to low solar activity, leading to a corresponding modulation in the thermosphere/ionosphere system (Kutiev et al., 2013).

The 27-day variations in solar and geomagnetic activity contribute significantly to the 27-day variations in the NmF2. However, the role of geomagnetic activity is complex. Ma et al. (2012) have studied the 27-day variations of NmF2 in detail using ionosonde observations. They show that the 27-day variations of solar irradiance and geomagnetic activity caused by the solar rotation are the main factors for the 27-day variations of the ionosphere. Apart from solar activity and geomagnetic activity, the 27-day variations in the lower ionosphere (D region), especially in winter when solar activity is low, are due to lower atmospheric influences (planetary waves) (Pancheva et al., 1991). But the D region contributes only weakly to the ionospheric electron density. There is a considerable influence of lower atmosphere waves (planetary waves, tides, and gravity waves) on the entire ionosphere, including TEC and NmF2. These effects are more prominent during solar maximum. In this article we focus on the fluctuations of NmF2 under different solar activity.

The relationship between solar flux and ionospheric parameters is important for monitoring and modeling solar variability in particular with respect to space weather applications, and has been studied by many researchers (e.g. Kane, 1992; Rishbeth, 1998; Forbes et al., 2000; Oinats et al., 2008; Astafyeva et al., 2008; Min et al., 2009; Ma

et al., 2012). An ionospheric lag of about 17 hours to 2 days in thermosphere-ionosphere parameters such as NmF2, TEC, temperature, and neutral densities with respect to solar EUV flux measurements and EUV proxies (e.g., F10.7 index, Mg-II index, etc.) has been extensively reported by various authors (e.g. Jakowski et al., 1991; Afraimovich et al., 2008; Liu and Chen, 2009; Unglaub et al., 2012; Chen et al., 2015; Jacobi et al., 2016; Vaishnav et al., 2019, 2021b; Schmölter et al., 2018, 2020, 2021, 2022; Ren et al., 2018, 2019, see also references therein), and it was reported that this lag may vary with solar activity and season.

The physical mechanism of ionospheric delay in TEC and neutrals against solar flux has been studied by several authors (e.g. Jakowski et al., 1991; Vaishnav et al., 2021a, 2022; Ren et al., 2018; Schmölter et al., 2022) by using numerical physics-based models such as the Coupled Thermosphere Ionosphere Plasmasphere electrodynamics (CTIPe, Fuller-Rowell and Rees, 1980) model, or the Thermosphere Ionosphere Electrodynamics-General Circulation Model (TIE-GCM, Richmond et al., 1992). The delay in the ionosphere is mainly due to the difference in response times between quasi-instantaneous ionization and slower recombination in the ionospheric F region (Ren et al., 2018). In addition, eddy diffusion, electrodynamics, and lower atmospheric forcings also influence the ionospheric delay (Vaishnav et al., 2021a). In addition to solar activity, geomagnetic activity may also play an important role in the ionospheric delay (Schmölter et al., 2020).

The present study aims to investigate the effects of 27-day variations in the peak electron density of the F2 region and solar and geomagnetic parameters in years of low (2008) and high (2013) solar activity. We also investigate an ionospheric delay in NmF2 during various solar activity conditions under ideal atmospheric conditions. In Section 2, we present our data sources, and the CTIPe model used for the analyses. In Section 3, we examine the 27-day variability of solar activity, geomagnetic activity, and NmF2, as well as the ionospheric delay under different solar activity conditions. Section 4 concludes the paper.

2 Data and model description

2.1 Data sources

The F10.7 solar radio flux is one of the most commonly used indices of solar activity (Tapping, 2013). We use the daily values of the F10.7 index. The F10.7 index values are available in the LISIRD database (Dewolfe et al., 2010). In addition, as a measure of geomagnetic activity, we used the daily Ap indices from the OMNIWeb Plus database (https://omniweb.gsfc.nasa.gov/, NASA, 2022).

2.2 FORMOSAT-3/COSMIC

The Constellation Observing System for Meteorology, Ionosphere, and Climate/Formosa Satellite Mission 3 (COSMIC/FORMOSAT-3, hereafter COSMIC) was a joint Taiwan U.S. occultation satellite mission, a constellation of six microsatellites launched on April 2006, initially in 500 km orbit and later in 800 km orbit and at an inclination of 72° (Anthes et al., 2008). COSMIC provides neutral and ionospheric parameters via the COSMIC Data Analysis and Archive Center (CDAAC).

In this study, electron density profiles (ionPrf) for 2008 and 2013 have been used (http://cdaacwww.cosmic.ucar.edu/cdaac/rest/tarservice/data/cosmic2013/ionPrf).

2.3 CTIPe model

The CTIPe model is a global, time-dependent model of the upper atmosphere that self-consistently solves the primitive continuity, momentum, and energy equations to calculate wind components, global temperature, and neutral composition, and which is also used to calculate plasma production, loss, and transport. The model consists of four components, namely a neutral thermosphere model (Fuller-Rowell and Rees, 1980), a mid- and high-latitude ionosphere convection model (Quegan et al., 1982), a plasmasphere and low-latitude ionosphere model (Millward et al., 1996), and an electrodynamics model (Richmond et al., 1992). Calculations are performed at a resolution of 2°/18° in latitude/longitude. In the vertical direction, the atmosphere is divided into 15 logarithmic pressure levels at an interval of one scale height, starting with a lower boundary at 1 Pa (about 80 km altitude) up to over 500 km altitude at pressure level 15. The model requires several external forcing factors such as solar UV and EUV radiation, Weimer electric field, TIROS /NOAA auroral precipitation, and tidal forcing at the lower boundary. The F10.7 index is used as a solar proxy to calculate ionization, heating, and oxygen dissociation in the ionosphere. A detailed description of the model can be found in Codrescu et al. (2008, 2012).

2.4 WACCM-X

The National Center for Atmospheric Research (NCAR) Whole Atmosphere Community Climate Model with thermosphere and ionosphere extension (WACCM-X) is a global numerical model of the entire atmosphere, from the surface to an altitude of about 600 km, depending on solar activity. The first version of WACCM-X was described by Liu et al. (2010). WACCM-X is an atmospheric component of the NCAR Community Earth System Model that links the atmosphere, ocean, land surface, sea ice, land ice, and carbon cycle components through flux and state information exchange (Hurrell et al., 2013). Recent extensions of WACCM-X include a fully coupled ionosphere, including electric field effects and ion transport. The vertical resolution in the mesosphere and thermosphere is one-quarter of a scale height and the horizontal resolution is 1.9°/2.5° in latitude and longitude, respectively. A detailed description of the new version (version 2.0) of WACCM-X can be found in Liu et al. (2018a).

3 Results

In this work, we focused on the variability of NmF2 during different solar activity conditions. For this purpose, we performed two types of model experiments. In the first experiment, we used more realistic atmospheric conditions from March and July 2008 and 2013, using the solar, geomagnetic, and other realistic inputs with the default model settings. The model simulations from the first experiment are used in Sections 3.1 and 3.2. The second experiment was conducted with only one day of constant atmospheric conditions on March 15, 2013, and we varied only F10.7 in an artificial manner for

a 27-day solar rotation period to observe the effects of solar flux. This experiment is described in more detail in Section 3.3. In general, we used ionospheric electron density profiles between 170 and 400 km to derive the peak election density NmF2.

3.1 NmF2 comparisons

Figure 1 shows maps of monthly mean NmF2 from COSMIC (top panel), WACCM-X (middle panel), and CTIPe (middle panel) in March and July 2008 and 2013. The white lines indicate the dip equator. Longitudinal and latitudinal variations are evident from the figure. The maximum of NmF2 is seen in the low latitude region around the dip equator. In general, the effect of solar activity can be seen in COSMIC NmF2 and is well reproduced in the WACCM-X and CTIPe models. In 2008, solar activity was very low, so the overall WACCM-X NmF2 was lower than in 2013, showing a strong dependence on solar activity. In addition, NmF2 is larger in March than in July. This feature is observed in both low and high solar activity years. This is due to the semi-annual fluctuations of NmF2 (e.g., Qian et al., 2013). In addition, NmF2 is higher in March in the Northern Hemisphere, while NmF2 is higher in July in the Southern Hemisphere. These variations are due to the winter-summer asymmetry of equatorial ionization anomalies (EIA) resulting from electrodynamic, thermodynamic, and chemical processes (e.g., Lin et al., 2007). Liu et al. (2018b) presented the new development of the WACCM-X. They showed that the climatological characteristics of the ionospheric peak densities and heights (NmF2 and hmF2) of WACCM-X are in general agreement with the results obtained from the COSMIC data. They also found that NmF2 values predicted by WACCM-X are smaller and EIA are closer to the magnetic equator than observations from COSMIC and ionosondes.

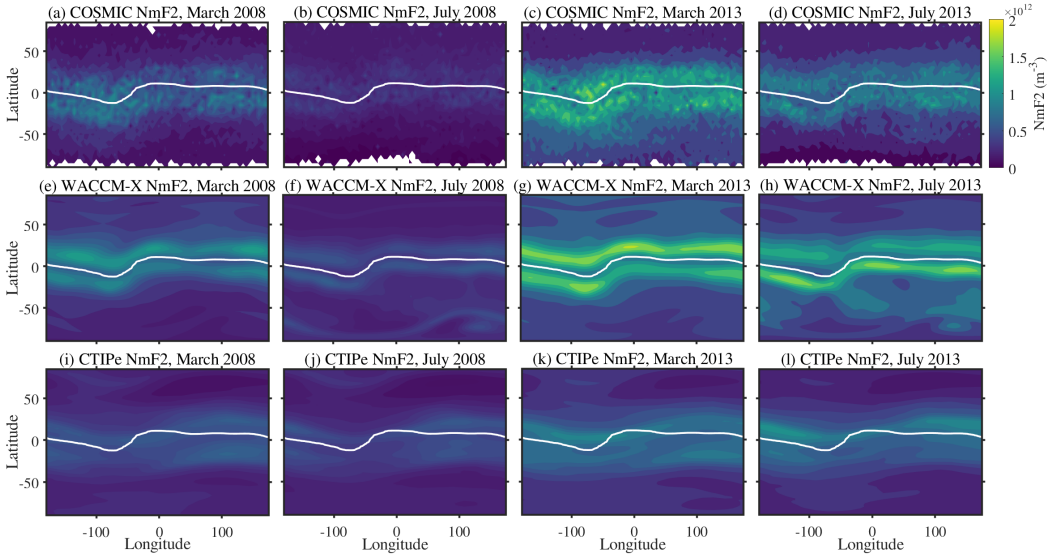

Figure 1: *Variations of NmF2 observed from COSMIC (a-d, upper panel), simulated with WACCM-X (e-h, lower panel), and with CTIPe (i-l, lower panel) during March and July 2008 and 2013. The month and year are indicated in the respective figure title. The white lines indicate the dip equator.*

The bottom panels in Figure 1(i-l) shows the NmF2 simulated by CTIPe. Compared

to the WACCM and COSMIC NmF2, the CTIPe NmF2 is generally lower. It lacks some climatological features clearly seen in the COSMIC and WACCM-X NmF2. The underestimation could be a consequence of the model limitations (e.g., grid resolution, and solar EUV flux input) highlighted by Codrescu et al. (2008, 2012). NmF2 varies with solar activity and also shows the slightly larger NmF2 in March compared to July indicates the semi-annual variations, as seen in COSMIC and WACCM-X NmF2, although they are not that clearly expressed in this model.

Diurnal variations of NmF2 as a function of time for the WACCM-X and CTIPe models in March and July 2008 and 2013 at $50°N/18°E$ are shown in Figure 2. The figure shows the monthly mean values of NmF2 with standard deviations. Most of the time CTIPe underestimates the WACCM-X NmF2, except in July 2008 from 10:00 UT to 14:00 UT as shown in Figure 2(b). The bias is due to the physical processes included in both CTIPe and WACCM-X models. The diurnal variations look similar in March of both years, except for the magnitude. The semi-annual variations can be seen in the figure, and the NmF2 values are larger in March than in July.

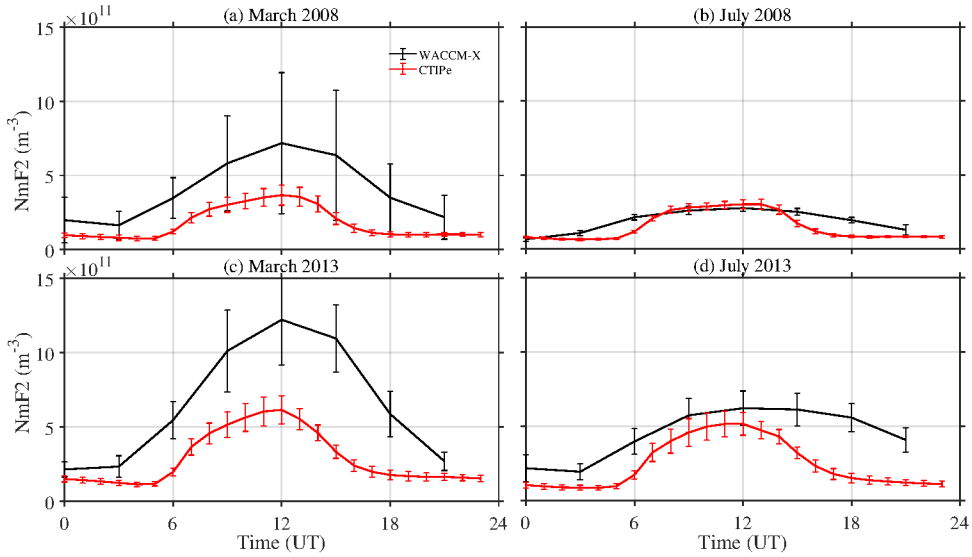

Figure 2: *Diurnal variations of mean NmF2 with standard deviation simulated with WACCM-X (upper panel) and CTIPe (lower panel) at* $50°N/18°E$ *during (a) March 2008, (b) July 2008, (c) March 2013, and (d) July 2013.*

3.2 The 27-day variations

We used the F10.7 index (Ap index) to represent solar (geomagnetic) activity. To focus only on the 27-day variations that represent the dominant oscillation in the solar proxies, we first performed a smoothing procedure similar to Ma et al. (2012). In this method, a 33 days moving average with one day step was calculated to isolate the 27-day variations. The relative changes can be determined using equation 1:

$$\Delta A_i = (A_i - \mu)/\mu. \tag{1}$$

A_i represents the time series of F10.7, Ap, and NmF2, and μ represents the 33 day moving averages of A_i. To focus only on the 27-day variations, we applied a bandpass

filter between 22 and 33 days to filter out the unfiltered ΔF10.7, ΔAp, and ΔNmF2 from Eq. 1, which we refer to below as the filtered time series (after bandpass filtering) and denote by Δ_{27}F10.7, Δ_{27}Ap, and Δ_{27}NmF2. The relative deviations of ΔF10.7 and ΔAp in 2008 and 2013 are shown in Figure 3. The gray (black) curve shows the unfiltered (filtered) deviations.

Figure 3(a-b) shows the deviations in the filtered and unfiltered time series of ΔF10.7. The ΔF10.7 and Δ_{27}F10.7 deviations show a similar response to the 27-day solar rotation period. The deviations are much larger during the high solar activity period than during the low solar activity period. It can also be seen that the 27-day variations are more pronounced in 2013. The deviations are weaker during June to August 2013. Since the period of solar rotation changes frequently, we cannot reconstruct the similar variations from the filtered time series (see Ma et al., 2012).

A similar analysis of the Ap index shows the 27-day variations in the filtered time series (Figure 3(d-e)). In 2008, the 27-day fluctuations are stronger than in 2013, and there are several short-term fluctuations in the Ap index that result in different dominant periods shorter than the 27-day fluctuations. We also performed a spectral analysis of ΔF10.7 and ΔAp (not shown). In ΔF10.7, the dominant period in 2008 and 2013 are 27 days. In ΔAp, the 27-day period is the dominant period, however shorter periods such as 13.5 days and 9 days are also present. These periods are dominant in 2008, while they are less so in 2013.

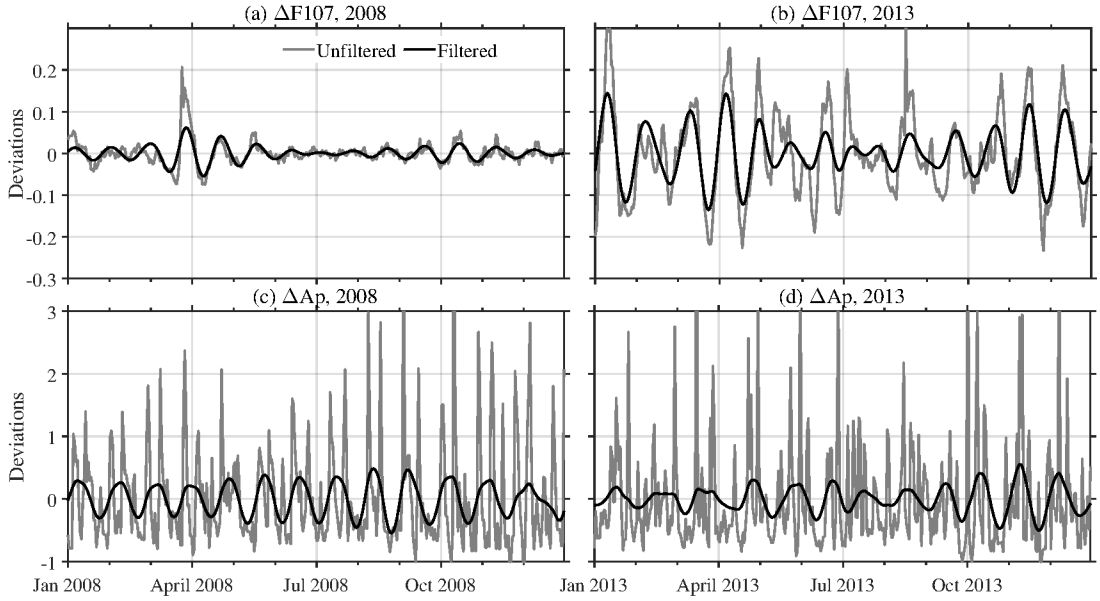

Figure 3: *The time series of unfiltered (gray) and filtered (black) relative deviations of the ΔF10.7 index (top panel, a-b) and ΔAp indices (bottom panel, c-d) during 2008 (left panel) and 2013 (right panel).*

Vaishnav et al. (2019) reported a dominant 27-day period in several solar proxies and TEC. This is the dominant mode of solar variability. Therefore, in this study, we examine the 27-day variations of CTIPe NmF2 at 0°/18°E, 30°N/18°E, and 30°S/18°E. We first performed the smoothing and filtering mentioned above to filter out the signal at periods longer than 33 days. To examine the difference between Δ_{27}NmF2 variations during low (2008) and high (2013) solar activity, we used averaged Δ_{27}NmF2 values.

Figure 4 shows the Δ_{27}NmF2 at the three grid points above for midday (11:00-13:00 LT) and midnight (23:00-01:00 LT) in low and high solar activity years along with the Δ_{27}F10.7. Figure 4(a-b) shows that in 2008, the changes in Δ_{27}NmF2 are larger at 30°S during both midday and midnight from July to October 2008, while the changes during midnight are larger at 0° from January to April 2008 and after October 2008. In Δ_{27}F10.7, the larger variation is observed in March-April. During this period, the variations are in phase with the lag during the midday period, and similar for the midnight period, except for 0°, which is 180° out of phase. Similarly, in May 2013, we found a phase deviation of 180° for 30°S with respect to Δ_{27}F10.7 during midday and midnight (Figure 4(b-d)). In 2013, the deviations for midday are larger at 0°, 30°N through April, and in November and December. In November-December, the deviations are again out of phase at 30°S with Δ_{27}F10.7 during midday and during midnight, similar holds for 0° and 30°S (Figure 4(d)).

Overall, the midnight Δ_{27}NmF2 variations are stronger than the midday ones. It is also interesting to note that at low solar activity the Δ_{27}NmF2 variations are larger at 30°S, while at high solar activity the Δ_{27}NmF2 variations are larger at 0° and 30°N during midday.

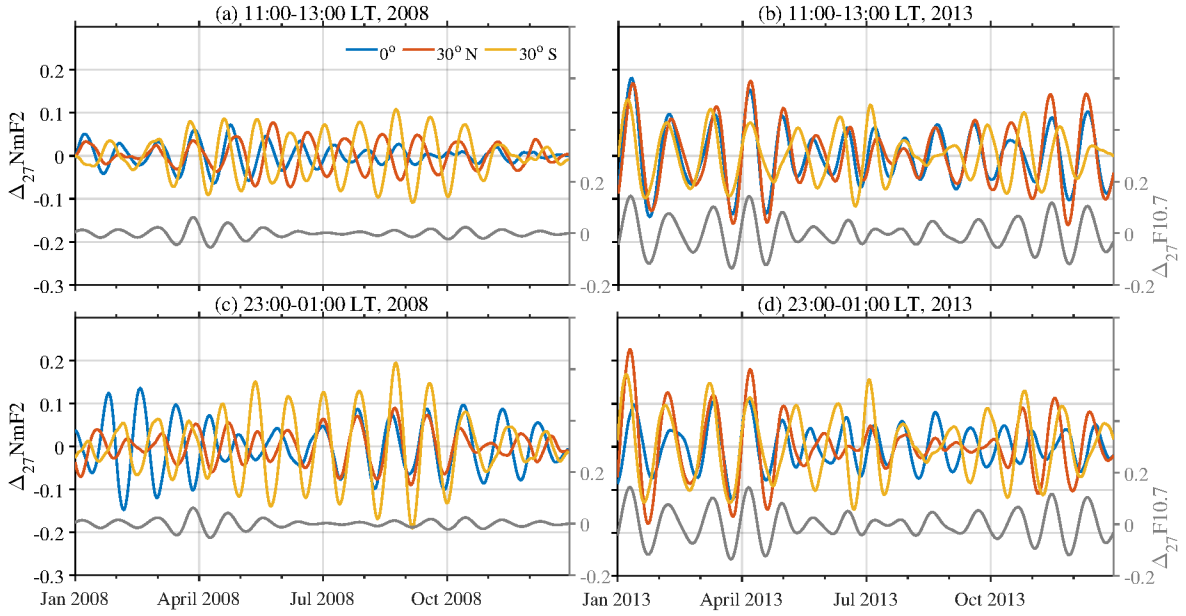

Figure 4: *Day to day variations of Δ_{27}NmF2 during 2008 (left panel, a-c) and 2013 (right panel, b-d). The upper (lower) panel shows the midday (midnight) variations at 0°/18°E, 30°N/18°E, and 30°S/18°E. The right y-axis represents the Δ_{27}F10.7 (gray curve).*

Ma et al. (2012) used 18 years of ionosonde data over 11 stations to examine the 27-day variations. They reported that the normalized standard deviation of the midnight 27-day variations of NmF2 is larger than that of midday, which is also observed for the Δ_{27}NmF2 simulated by CTIPe. They also suggest that the 27-day solar rotation is the main cause of the 27-day variations in the ionosphere.

3.3 Ionospheric delay in NmF2 under different solar activity conditions

An ionospheric lag compared to solar flux has been found in various ionospheric parameters (e.g. Jakowski et al., 1991; Liu and Chen, 2009; Jacobi et al., 2016; Vaishnav et al., 2019, 2022; Schmölter et al., 2020, 2022; Ren et al., 2018, and references therein). Overall, recent studies using physics based numerical models of the global thermosphere-ionosphere suggest that the ionospheric delay process is influenced by several factors, including solar, geomagnetic, and electrodynamic ones, eddy diffusion, and lower atmospheric forcings.

In this work, we focus on the study of the ionospheric delay in NmF2 to solar irradiance. For this purpose, we performed two experiments with the CTIPe model simulations in different ranges of the F10.7 index at a cycle of 27 days under ideal conditions. The model was run for 30 days with input parameters held constant to achieve diurnal reproducibility, and inputs were changed after this spin-up period. We used constant atmospheric conditions for March 15, 2013, and ran the model varying the F10.7 index for the 27-day solar rotation period. The F10.7 index was chosen for low (70-90 sfu) and high (150-190 sfu) solar activity. We calculated the time delay using the hourly simulated NmF2 and F10.7. The F10.7 index was interpolated to hourly data using a sine function (Vaishnav et al., 2021a).

Figure 5 shows the daily variations of NmF2 (black curve) during (a) low and (b) high solar activity together with the F10.7 index (gray curve) at $50°N$. The figure shows that NmF2 follows solar activity in the ascending phase of the solar rotation period and increases with solar activity. In the descending phase of the solar rotation period, the behaviour of NmF2 changes and NmF2 does not return to the initial values, which is due to the imbalance of the production and loss processes of electrons in the F2 region. Further, the ionospheric delay in NmF2 is calculated using the F10.7 index and shown in the figure. The ionospheric delay at low solar activity is about 12 hours, as shown in Figure 5(a). After the zero day, the recombination processes are balanced by the photoionization rates, resulting in a delay of about 12 hours. Compared to low solar activity, an ionospheric delay of about 34 hours is observed at high solar activity (Figure 5(b)). Again, the values of NmF2 do not return to initial values after a complete cycle, and the difference between the production and loss processes is much larger, leading to a longer delay compared to low solar activity. This suggests that solar activity plays an important role in the ionospheric delay of NmF2, and the ionospheric delay increases with increasing solar activity.

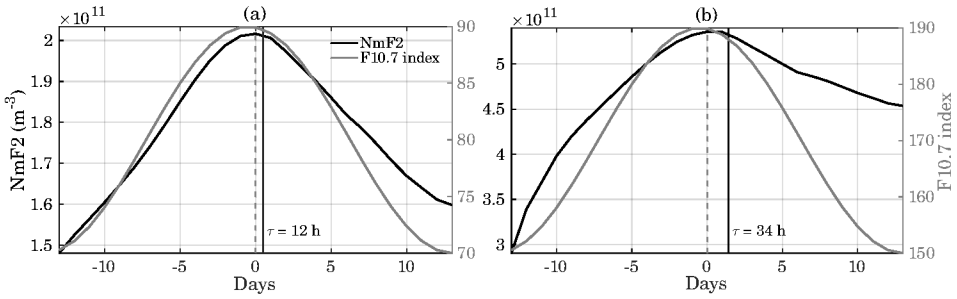

Figure 5: *Time series of model-simulated NmF2 during (a) low (70-90 sfu), and (b) high (150-190 sfu) solar activity. The right y-axis represents the input F10.7 index.*

4 Conclusions

We studied the ionospheric response to solar variability using the CTIPe simulated ionospheric peak electron density NmF2 for 2008 and 2013 under low and high solar activity conditions. The CTIPe NmF2 was compared to the observed COSMIC and the modeled WACCM-X NmF2 in March and July of 2008 and 2013. The CTIPe NmF2 is lower than the COSMIC and WACCM-X NmF2 during the periods studied. Both models successfully reproduce the semi-annual variations that can be seen in the COSMIC NmF2.

The CTIPe model simulated NmF2 was used to examine the 27-day fluctuations at $0°/18°E$, $30°N/18°E$, and $30°S/18°E$. We found that the 27-day variations in midnight NmF2 are stronger than the midday variations, which is consistent with observations. The analysis also shows that at low solar activity the 27-day variations of NmF2 are larger at $30°S$, while at high solar activity the 27-day variations of NmF2 are larger at $0°$ and $30°N$ during midday.

In addition, the ionospheric delay was estimated with the model simulated NmF2 during low and high solar activity. An ionospheric delay of about 12 hours is observed during low solar activity and 34 hours during high solar activity. This shows that the ionospheric delay increases with increasing solar activity.

Here, we discussed the 27-day variations of NmF2 at low (2008) and high (2013) solar activity and focused on the ionospheric delay of NmF2 at moderate and high solar activity. In future studies, we will further investigate the effects and main roles of the different processes affecting the ionospheric delay and their physical mechanisms using modelling and observations. In addition, the 27-day variations in solar activity and geomagnetic activity contribute to the 27-day variations in peak electron density (NmF2). Therefore, further studies are needed to understand the complexity of these factors and their role in the delayed ionospheric response.

Acknowledgements Daily F10.7 index and Ap index can be downloaded from https://omniweb.gsfc.nasa.gov/ (NASA, 2022). The study has been supported by Deutsche Forschungsgemeinschaft (DFG) through grants nos. JA 836/48-1 and SCHM 3761/1-1.

References

Afraimovich, E. L., Astafyeva, E. I., Oinats, A. V., Yasukevich, Y. V., and Zhivetiev, I. V.: Global electron content: a new conception to track solar activity, Annales Geophysicae, 26, 335–344, doi:10.5194/angeo-26-335-2008, 2008.

Anthes, R. A., Bernhardt, P. A., Chen, Y., et al.: The COSMIC/FORMOSAT-3 Mission: Early Results, Bulletin of the American Meteorological Society, 89, 313–334, doi:10.1175/bams-89-3-313, 2008.

Astafyeva, E. I., Afraimovich, E. L., Oinats, A. V., Yasukevich, Y. V., and Zhivetiev, I. V.: Dynamics of global electron content in 1998-2005 derived from global GPS data and IRI modeling, Advances in Space Research, 42, 763–769, doi:10.1016/j.asr.2007.11.007, 2008.

Chen, Y., Liu, L., Le, H., and Zhang, H.: Discrepant responses of the global electron content to the solar cycle and solar rotation variations of EUV irradiance, Earth, Planets and Space, 67, doi:10.1186/s40623-015-0251-x, 2015.

Codrescu, M. V., Fuller-Rowell, T. J., Munteanu, V., Minter, C. F., and Millward, G. H.: Validation of the

Coupled Thermosphere Ionosphere Plasmasphere Electrodynamics model: CTIPE-Mass Spectrometer Incoherent Scatter temperature comparison, Space Weather, 6, doi:10.1029/2007sw000364, 2008.

Codrescu, M. V., Negrea, C., Fedrizzi, M., et al.: A real-time run of the Coupled Thermosphere Ionosphere Plasmasphere Electrodynamics (CTIPe) model, Space Weather, 10, doi:10.1029/2011sw000736, 2012.

Dewolfe, A. W., Wilson, A., Lindholm, D. M., et al.: Solar Irradiance Data Products at the LASP Interactive Solar Irradiance Datacenter (LISIRD), in: AGU Fall Meeting Abstracts, 2010.

Forbes, J. M., Palo, S. E., and Zhang, X.: Variability of the ionosphere, Journal of Atmospheric and Solar-Terrestrial Physics, 62, 685–693, doi:10.1016/s1364-6826(00)00029-8, 2000.

Fuller-Rowell, T. J. and Rees, D.: A Three-Dimensional Time-Dependent Global Model of the Thermosphere, Journal of the Atmospheric Sciences, 37, 2545–2567, doi:10.1175/1520-0469(1980)037<2545:atdtdg>2.0.co;2, 1980.

Hurrell, J. W., Holland, M. M., Gent, P. R., et al.: The Community Earth System Model: A framework for collaborative research, Bulletin of the American Meteorological Society, 94, 1339–1360, doi:10.1175/bams-d-12-00121.1, 2013.

Jacobi, C., Jakowski, N., Schmidtke, G., and Woods, T. N.: Delayed response of the global total electron content to solar EUV variations, Advances in Radio Science, 14, 175–180, doi:10.5194/ars-14-175-2016, 2016.

Jakowski, N., Fichtelmann, B., and Jungstand, A.: Solar activity control of ionospheric and thermospheric processes, Journal of Atmospheric and Terrestrial Physics, 53, 1125–1130, doi:10.1016/0021-9169(91)90061-B, 1991.

Kane, R. P.: Sunspots, solar radio noise, solar EUV and ionospheric foF2, Journal of Atmospheric and Terrestrial Physics, 54, 463–466, doi:10.1016/0021-9169(92)90025-G, 1992.

Kutiev, I., Tsagouri, I., Perrone, L., et al.: Solar activity impact on the Earth's upper atmosphere, Journal of Space Weather and Space Climate, 3, A06, doi:10.1051/swsc/2013028, 2013.

Lin, C. H., Liu, J. Y., Fang, T. W., et al.: Motions of the equatorial ionization anomaly crests imaged by FORMOSAT-3/COSMIC, Geophysical Research Letters, 34, L19 101, doi:10.1029/2007gl030741, 2007.

Liu, H.-L., Foster, B. T., Hagan, M. E., et al.: Thermosphere extension of the Whole Atmosphere Community Climate Model, Journal of Geophysical Research: Space Physics, 115, A12 302, doi:10.1029/2010ja015586, 2010.

Liu, H.-L., Bardeen, C. G., Foster, B. T., et al.: Development and Validation of the Whole Atmosphere Community Climate Model With Thermosphere and Ionosphere Extension (WACCM-X 2.0), Journal of Advances in Modeling Earth Systems, 10, 381–402, doi:10.1002/2017ms001232, 2018a.

Liu, J., Liu, H., Wang, W., et al.: First Results From the Ionospheric Extension of WACCM-X During the Deep Solar Minimum Year of 2008, Journal of Geophysical Research: Space Physics, 123, 1534–1553, doi:10.1002/2017ja025010, 2018b.

Liu, L. and Chen, Y.: Statistical analysis of solar activity variations of total electron content derived at Jet Propulsion Laboratory from GPS observations, Journal of Geophysical Research: Space Physics, 114, doi:10.1029/2009ja014533, 2009.

Ma, R., Xu, J., Wang, W., and Lei, J.: The effect of ~27 day solar rotation on ionospheric F2 region peak densities (NmF2), Journal of Geophysical Research: Space Physics, 117, A03 303, doi:10.1029/2011ja017190, 2012.

Millward, G., Moffett, R., Quegan, S., and Fuller-Rowell, T.: A coupled thermosphere-ionosphere-plasmasphere model (CTIP), STEP handbook on ionospheric models, pp. 239–279, 1996.

Min, K., Park, J., Kim, H., et al.: The 27-day modulation of the low-latitude ionosphere during a solar maximum, Journal of Geophysical Research: Space Physics, 114, 1–8, doi:10.1029/2008JA013881, 2009.

NASA: OMNIWeb Plus database, available at: `http://omniweb.gsfc.nasa.gov/`, last access: 15 April 2022, 2022.

Oinats, A. V., Ratovsky, K. G., and Kotovich, G. V.: Influence of the 27-day solar flux variations on the ionosphere parameters measured at Irkutsk in 2003-2005, Advances in Space Research, 42, 639–644, doi:10.1016/j.asr.2008.02.009, 2008.

Pancheva, D., Schminder, R., and Laštovička, J.: 27-day fluctuations in the ionospheric D-region, Journal

of Atmospheric and Terrestrial Physics, 53, 1145–1150, doi:10.1016/0021-9169(91)90064-e, 1991.

Qian, L., Burns, A. G., Solomon, S. C., and Wang, W.: Annual/semiannual variation of the ionosphere, Geophysical Research Letters, 40, 1928–1933, doi:10.1002/grl.50448, 2013.

Quegan, S., Bailey, G. J., Moffett, R. J., et al.: A theoretical study of the distribution of ionization in the high-latitude ionosphere and the plasmasphere: first results on the mid-latitude trough and the light-ion trough, Journal of Atmospheric and Terrestrial Physics, 44, 619–640, doi:10.1016/0021-9169(82)90073-3, 1982.

Ren, D., Lei, J., Wang, W., et al.: Does the Peak Response of the Ionospheric F2 Region Plasma Lag the Peak of 27-Day Solar Flux Variation by Multiple Days?, Journal of Geophysical Research: Space Physics, pp. 1–11, doi:10.1029/2018JA025835, 2018.

Ren, D., Lei, J., Wang, W., et al.: A Simulation Study on the Time Delay of Daytime Thermospheric Temperature Response to the 27-Day Solar EUV Flux Variation, Journal of Geophysical Research: Space Physics, 124, 9184–9193, doi:10.1029/2019ja027000, 2019.

Richmond, A. D., Ridley, E. C., and Roble, R. G.: A thermosphere/ionosphere general circulation model with coupled electrodynamics, Geophysical Research Letters, 19, 601–604, doi:10.1029/92GL00401, 1992.

Rishbeth, H.: How the thermospheric circulation affects the ionospheric F2-layer, Journal of Atmospheric and Solar-Terrestrial Physics, 60, 1385–1402, doi:10.1016/s1364-6826(98)00062-5, 1998.

Schmölter, E., Berdermann, J., Jakowski, N., Jacobi, C., and Vaishnav, R.: Delayed response of the ionosphere to solar EUV variability, Advances in Radio Science, 16, 149–155, doi:10.5194/ars-16-149-2018, 2018.

Schmölter, E., Berdermann, J., Jakowski, N., and Jacobi, C.: Spatial and seasonal effects on the delayed ionospheric response to solar EUV changes, Annales Geophysicae, 38, 149–162, doi:10.5194/angeo-38-149-2020, 2020.

Schmölter, E., Berdermann, J., and Codrescu, M.: The Delayed Ionospheric Response to the 27-day Solar Rotation Period Analyzed With GOLD and IGS TEC Data, Journal of Geophysical Research: Space Physics, 126, doi:10.1029/2020ja028861, 2021.

Schmölter, E., Heymann, F., Savigny, C., and Berdermann, J.: The Height-Dependent Delayed Ionospheric Response to Solar EUV, Journal of Geophysical Research: Space Physics, 127, doi:10.1029/2021ja030118, 2022.

Tapping, K. F.: The 10.7 cm solar radio flux (F10.7), Space Weather, 11, 394–406, doi:10.1002/swe.20064, 2013.

Unglaub, C., Jacobi, C., Schmidtke, G., Nikutowski, B., and Brunner, R.: EUV-TEC proxy to describe ionospheric variability using satellite-borne solar EUV measurements, Advances in Radio Science, 10, 259–263, doi:10.5194/ars-10-259-2012, 2012.

Vaishnav, R., Jacobi, C., and Berdermann, J.: Long-term trends in the ionospheric response to solar extreme-ultraviolet variations, Annales Geophysicae, 37, 1141–1159, doi:10.5194/angeo-37-1141-2019, 2019.

Vaishnav, R., Jacobi, C., Berdermann, J., Codrescu, M., and Schmölter, E.: Role of eddy diffusion in the delayed ionospheric response to solar flux changes, Annales Geophysicae, 39, 641–655, doi:10.5194/angeo-39-641-2021, 2021a.

Vaishnav, R., Schmölter, E., Jacobi, C., Berdermann, J., and Codrescu, M.: Ionospheric response to solar extreme ultraviolet radiation variations: comparison based on CTIPe model simulations and satellite measurements, Annales Geophysicae, 39, 341–355, doi:10.5194/angeo-39-341-2021, 2021b.

Vaishnav, R., Jacobi, C., Berdermann, J., Schmölter, E., and Codrescu, M.: Delayed ionospheric response to solar extreme ultraviolet radiation variations: A modeling approach, Advances in Space Research, 69, 2460–2476, doi:10.1016/j.asr.2021.12.041, 2022.

Woods, T., Bailey, S., Eparvier, F., et al.: TIMED Solar EUV experiment, Physics and Chemistry of the Earth, Part C: Solar, Terrestrial & Planetary Science, 25, 393–396, doi:10.1016/s1464-1917(00)00040-4, 2000.